LA-UR- 94-269

Title: LAHET CODE SYSTEM/CINDER '90 CALIDATION CALCULATIONS AND COMPARISON WITH EXPERIMENTAL DATA

Author(s): G. Russell, T. O. Brun, C. A. Beard, L. L. Daemen, E. J. Pitcher, G. J. Russell, and W. B. Wilson

Submitted to: ICANS-XII, Abingdon, Oxforshire, UK
May 24-28, 1993

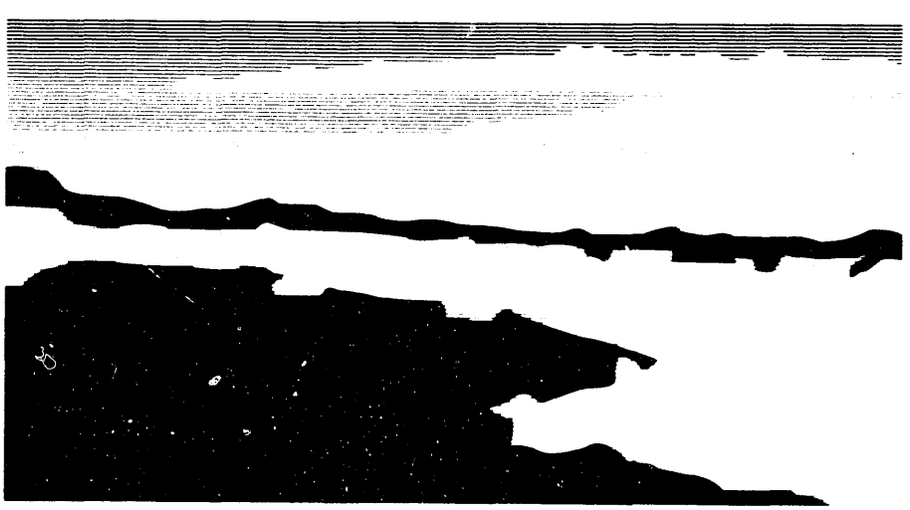

Los Alamos
NATIONAL LABORATORY

Form No. 836 R5
ST 2629 10/91

Twelfth Meeting of the International Collaboration on Advanced Neutron Sources
24-28 May 1993, The Cosener's House, Abingdon, Oxfordshire, U.K.

LAHET Code System/CINDER'90 Validation Calculations and Comparison With Experimental Data

T. O. Brun, C. A. Beard, L. L. Daemen, E. J. Pitcher, G. J. Russell, and W. B. Wilson
Los Alamos National Laboratory
Los Alamos, NM U.S.A.

We use the Los Alamos LAHET Code System (LCS)/CINDER'90 suite of codes in a variety of spallation neutron source applications to predict neutronic performance and as a basis for making engineering decisions. We have broadened our usage of the suite from designing LANSCE and the next generation of spallation neutron sources for materials science and nuclear physics research to designing a target system for Accelerator Production of Tritium and Accelerator Transmutation of Waste. While designing, we continue to validate the LCS/CINDER'90 code suite against experimental data whenever possible. In the following, we discuss comparisons between calculations and measurements for: integral neutron yields from a bare-target of lead; fertile-to-fissile conversion yields for thorium and depleted uranium targets; dose rates from the LANSCE tungsten target; energy deposition in a variety of light and heavy materials; and neutron spectra from LANSCE water and liquid hydrogen moderators. The accuracy with which our calculations reproduce experimental results is an indication of our confidence in the validity of our design calculations.

Introduction

At Los Alamos, we have world-class Monte Carlo computational capability, which can be used for a variety of spallation-neutron-source design applications in environments with requisite computer hardware and experienced people to set up and run the codes and interpret the results. One part of our computational tool is based on the LANL version of the HETC Monte Carlo code for the transport of nucleons, pions, and muons, which was originally developed at ORNL [1]. Because of major modifications and additions made to the HETC code at LANL, our version of HETC has been renamed LAHET, and the system of codes based on LAHET (which we use in spallation neutron source design) is designated the LAHET Code System (LCS) [2]. The LCS is a sophisticated code system based on several sub-components, among which LAHET and the Los Alamos continuous energy neutron, photon, electron monte carlo code MCNP are the major players. CINDER'90 describes the temporal concentrations of nuclides depleted and produced in materials subject to spallation and neutron reactions [3].

In the following, we offer a brief description of the LCS and CINDER'90 codes and indicate the breadth of capabilities that this suite of codes puts at the users' disposal. We compare calculated predictions to measured values for a variety of "benchmark" experiments including

- integral neutron leakage from lead targets bombarded by protons with energies from 800 MeV to 3 GeV;
- fertile-to-fissile conversion yields for bare targets of thorium and depleted uranium bombarded by 800-MeV protons;
- neutron dose rates from the LANSCE tungsten target;
- energy deposition in a variety of target materials as a function of proton energy; and
- neutron spectra from the LANSCE water and liquid hydrogen moderators.

Calculational Methodology

Overview of the LAHET Code System

Group X–6 at LANL develops, maintains, and supports the LCS and distributes the code system worldwide. LAHET itself is used for the transport and interaction of nucleons, pions, and muons at high-energies (20 MeV<E<~4 GeV). LAHET uses the Bertini [4] or the ISABEL [5] model to describe the physics of the intranuclear cascade and uses the Dresner evaporation model [6] for the last phase of the nuclear interaction. (The Fermi breakup model [7] replaces the Dresner model for describing the evaporation process for light nuclei.) Group X–6 recently added a preequilibrium model [8] as an intermediate stage between the intranuclear phase and the evaporation phase; two fission models (Rutherford-Appleton [9] or ORNL [10]) complement the set of physics models LAHET uses.

The MCNP code (developed at LANL over the past 40 years or so) is a design-production code for low-energy neutron/photon/electron Monte Carlo transport [11]. The code is distributed and used internationally by nuclear-systems designers. The MCNP code is geared toward the transport of neutrons, photons, and electrons in matter and uses very detailed cross sections for several hundred isotopes to describe the interaction of neutrons and photons with matter down to thermal energies. MCNP makes use of ENDF/B–V cross section for neutron and photon reactions. We describe thermal neutron reactions using the free gas model or, when available, detailed scattering kernels, the $S(\alpha,\beta)$ treatment. For photons, the code takes coherent and incoherent scattering, fluorescent emission after photoelectric absorption, and various other physical processes into account. Contrary to multigroup codes, MCNP is a general-purpose, continuous-energy, generalized-geometry, and time-dependent Monte Carlo transport code. It is capable of handling arbitrarily complex three-dimensional geometries. The output MCNP produces ranges from neutron and gamma-ray fluxes and currents to energy deposition; from energy fluxes to gas production; and from radiation doses to criticality eigenvalues.

Particle transport in both LAHET and MCNP is based on Monte Carlo techniques. The philosophy used in the LAHET code is to treat all interactions by protons, pions, and muons within LAHET but to treat neutron interactions only above a cutoff energy, typically 20 MeV, at Los Alamos. Any low-energy (<20 MeV) neutron emerging from a reaction has its kinematic parameters recorded on a neutron file (NEUTP) for subsequent transport. For LAHET, a version of MCNP (called HMCNP) has been modified to accept the NEUTP file as an input source to complete the low-energy neutron transport using continuous-energy, ENDF/B-based, neutron cross-section libraries. Low-energy transported neutrons can participate in nuclear reactions and produce additional particles.

During a LAHET calculation, we record a large quantity of information on a separate file, which another piece of code, PHT—a photon source generating code—can subsequently analyze to produce a source for HMCNP. We can then execute the HMCNP phase of the calculation as a coupled neutron/photon transport problem. The photons originate either from the decay of neutral pions produced in the intranuclear cascade phase or by the deexcitation of residual nuclei after the evaporation phase. In a coupled neutron/photon problem, we merge the neutron file NEUTP and the gamma-ray file GAMTP (by the MRGNTP code in the LCS) to produce a combined neutron/photon file COMTP that describes the low-energy neutron source and high-energy-produced gamma-ray source for the entire system. We then use HMCNP to transport these neutrons and photons plus gamma rays produced from neutron-induced reactions below 20 MeV. In addition, both LAHET and HMCNP can write history files, called HISTP and HISTX, respectively, that contain a (nearly) complete description of events occurring during the computations. We postprocess the HISTP and HISTX files with another code (in the LCS suite of codes) called HTAPE. The edit options available with HTAPE include surface current and flux; cell-average neutron flux particle production spectra; residual mass production; mean excitation

energy; mass-energy balance, gas production and energy deposition by cell or material; pulse shape analysis of surface current; and global emission spectrum in polar and azimuthal bins.

The relationships of the various codes in the LCS and the files that carry information from one to another are shown in Figure 1. We use the LCS for a variety of applications including Spallation Neutron Source Design, Accelerator Production of Tritium (APT), and Accelerator Transmutation of Waste (ATW).

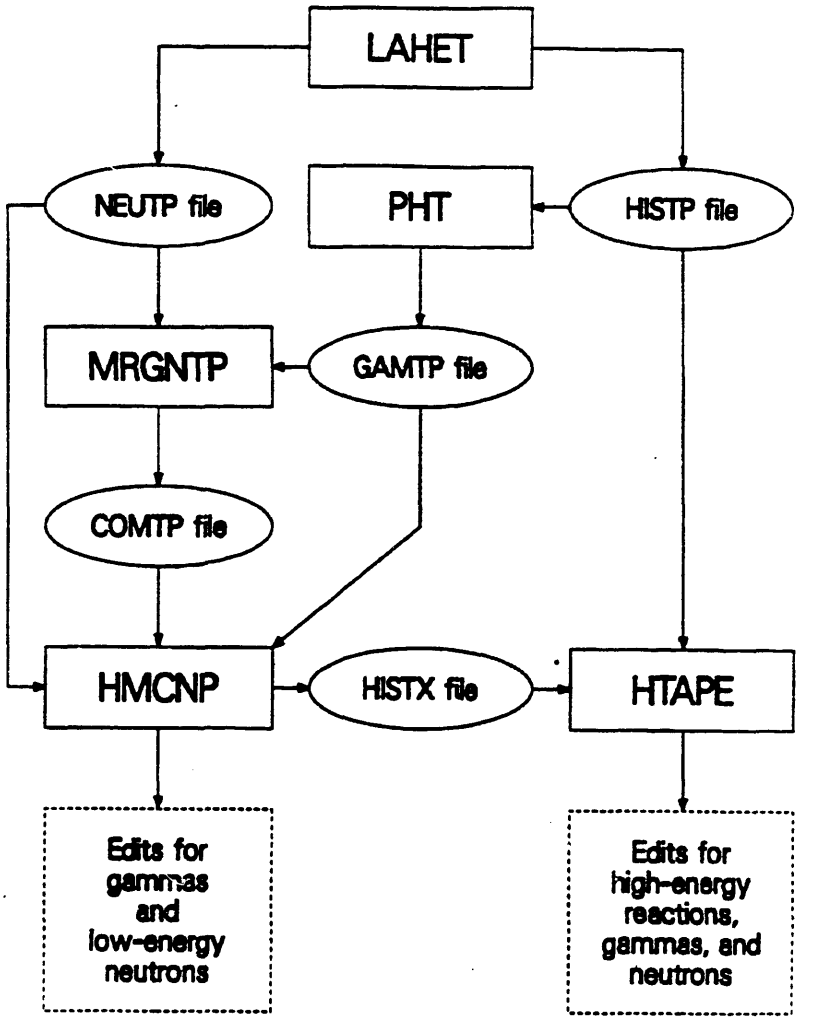

Fig. 1. LCS codes and data files.

Overview of CINDER'90

We describe the temporal concentrations of nuclides depleted and produced in materials subject to irradiation by a large set of coupled differential equations; and we determine each nuclide's concentration by a history of gains from neutron absorption reactions [spallation, fission, (n,γ), (n,2n), etc.] and radioactive decay of parent nuclides, as well as losses from its own decay and particle absorption. The solution for these nuclide concentrations was simplified in 1962 with the CINDER code, which resolved the complicated nuclide couplings into linear chains, each chain representing a unique path from nuclide to nuclide, resulting in small independent sets of

differential equations describing the rate of change of partial concentrations of nuclides in each chain. This reduces the solution of a large set of coupled differential equations to the solution of a number of small sets of differential equations, each characterized by a single generalized form. Because of the linear nature of the chain (a result of the Markov process), we may solve the generalized equations sequentially for the partial concentration of each linear nuclide in the chain. We then obtain nuclide concentrations by summing partial concentrations.

Calculations of radionuclide inventories in high-current, medium- and high-energy accelerator targets have required the development of a new inventory code (CINDER'90), evolved from earlier versions of CINDER [3, 12 through 16] and REAC, [17 through 20] and continuing development of cross-section and decay data. CINDER'90 uses these data with problem-specific spallation production and neutron-flux data calculated using LCS.

The CINDER'90 code differs from earlier CINDER versions in that earlier versions required the development of a library of transmutation chains before a calculation. Users selected chains of such libraries to follow transmutation paths that the user considered necessary and sufficient for the problem, and chains developed for one problem were not necessarily applicable to others. The CINDER'90 code uses a library of basic nuclear data to trace all possible transmutation paths, determining the partial concentration and associated activity of each linear nuclide as well as the integrated transmutation of each linear nuclide during a time increment. A linear nuclide's integrated transmutation, called the passerby, indicates the sum of subsequent partial concentrations in chains continuing from the nuclide. CINDER'90 examines each linear nuclide's partial concentration, activity, and passerby to determine whether a chain should be terminated relative to input significance criteria.

CINDER'90 accumulates nuclide concentrations and activities from linear nuclide properties as they are calculated. It then combines the postprocessing data with decay and neutron absorption data to obtain density (atoms/barn-cm and kg); activity (Ci/cm^3 and Ci); decay power (W/cm^3 and watts); macroscopic neutron absorption (cm^{-1}); and decay spectra properties listed by nuclide, element Z, and mass A. The code also tabulates major contributors ($\geq$0.1%) to mass, activity, decay power, and macroscopic absorption.

Many applications of these calculations are addressed with the direct utilization of the individual-nuclide and aggregate results—activity inventory, decay power, macroscopic neutron absorption, etc. Some applications require the tranport of the decay source γ's to obtain a desired response, such as dose or dose-equivalent rates.

Since target activity and nuclei inventory are very important for evaluating personnel safety risks and environmental impact of waste stream from a spallation target, the capability of predicting target activation and waste stream is extremely useful for target operations. Some applications require the transport of the decay source to obtain a desired response, such as dose or dose-equivalent rates. Transmutation calculation results are, of course, limited in accuracy by appropriate problem definition and by the validity of the nuclear data used in the calculation (i.e., neutron-absorption cross sections, decay constants for each nuclide transmutation path, and associated branching fractions to ground and isomeric states produced). Additional data describing the energy spectra and toxicity associated with the decay of radionuclides are required. The collection, calculation, and evaluation of the data are ongoing efforts currently involving dozens of scientists internationally. A detailed description of current CINDER'90 development activities is given in References 21 and 22.

Comparison between LCS Calculations and Experimental Data

The LAHET Code System is used worldwide for a variety of spallation neutron source applications. It is a premier design tool. As such, we must continue to evaluate the LCS against all types of basic and applied experimental data. The accuracy with which our calculations

reproduce experimental results is an indication of our confidence in the validity of our design calculations. We discuss below several comparisons we have made between LCS/CINDER'90 calculations and a variety of experimental data.

Bare-Target Integral Neutron Leakage

A simple test for the LAHET Code System consists of estimating neutron yields from simple targets. This particular test, although straightforward, is very important because it relates directly to the ability of LCS to reliably predict absolute neutron yields in the energy range of interest for spallation source applications. Other tests, even more stringent in nature, are described in subsequent sections.

Recent measurements by Vassilkov, et al. [23] in Dubna define an excellent test problem for LCS. They measured absolute neutron yields from a thick cylindrical lead target at various proton beam energies. More precisely, the target was a natural lead cylinder, 20 cm in diameter and 60 cm long. The JINR synchrocylotron in Dubna was used to produce a focused proton beam at various energies ranging from 990 to 3650 MeV. The proton beam characteristics are not known with great accuracy. In all our calculations, we assumed a circular, centered beam spot on target with the beam spot having a full width at half-maximum of 20 to 30 mm. In the experiment, absolute neutron yields were measured with threshold fission detectors.

Our simulations of the experiment with LAHET made use of the Bertini intranuclear cascade model followed by the application of a multistage preequilibrium model. This phase was in turn followed by the application of the Dresner evaporation model. The use and interfacing of these different models is not very crucial for total-yield calculations but could affect the details of the emission spectrum, for instance. Figure 2 shows the results produced by LCS, as well as the experimental data of Vassilkov, et al. Clearly, the agreement between the LCS results and the

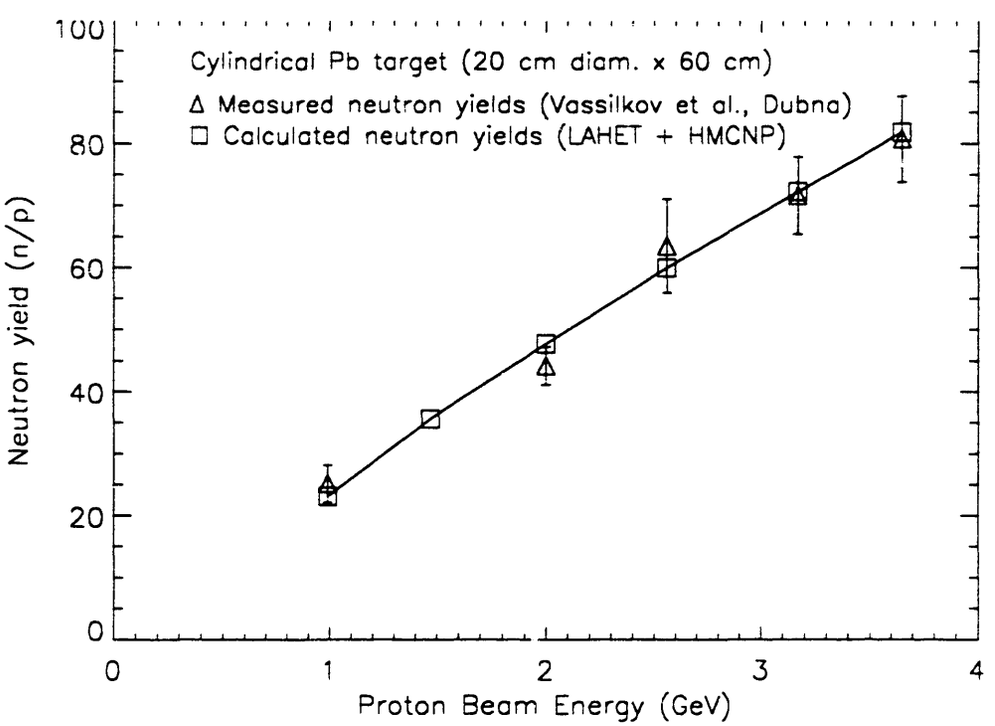

Fig. 2. Absolute neutron yields from a cylindrical (stopping length) Pb target 20 cm diam. × 60 cm long. Squares denote LCS results; triangles denote experimental results by Vassilkov, et al. The solid line is placed to guide the eye.

experimental data over the entire energy range is excellent, using models and parameters for those models that are the same as for our standard design calculations.

Los Alamos FERFICON Conversion Measurements

As part of the Fertile-to-Fissile Conversion program [24] at LANL, we measured the axial distributions of fissions and of fertile-to-fissile conversions in thick depleted uranium and thorium targets bombarded by 800-MeV protons. Table 1 gives the physical characteristics of the targets, and Fig. 3 illustrates the clustered target arrangements used in the experiments. We determined ^{239}Pu production from the amount of ^{239}Np formed and ^{233}U production from the amount of ^{233}Pa formed. We deduced the number of fissions from fission product mass-yield curves. We integrated the axial distributions to get the total number of conversions and fissions occurring in the targets. Table 2 shows measured conversion results compared to calculated predictions. The results are gratifying and indicate that the "source term" for low-energy (<20 MeV) neutron production is being handled well by LAHET. We are repeating the calculation with the latest model-values being used in LAHET.

Table 1 Physical Characteristics of the Targets

Material	Number of Rods	Density (g/cm^2)	Diameter (cm)	Length (cm)
Depleted Uranium*	37	19.04	19.70**	30.46
Thorium	19	11.38	18.28***	36.31

*0.251 wt% ^{235}U.

**Effective diameter of the clustered target ($D=d\sqrt{n}$) with an individual rod diameter of 3.239 cm.

***Effective diameter of the clustered target with an individual rod diameter if 4.194 cm.

Table 2 Comparison of Measured and Calculated Conversions for Thorium and Depleted Uranium Targets Bombarded by 800-MeV Protons

Target	Measured Conversion (atoms/protons)	Calculated Conversion (atoms/protons)
Thorium	1.25 ± 0.01	1.27 ± 0.01
Depleted Uranium	3.81 ± 0.01	3.88 ± 0.03

Russian Energy Deposition Measurements

Because we based our ^{3}He target/blanket system thermal-hydraulic design on calculated energy deposition, it is one of the most important pieces of information transferred to the engineering task. To estimate the accuracy of the LCS with regard to energy deposition, we compared LCS predictions with experimental results of Belyakov-Bodin, et al. [25-27]. We performed these comparisons for protons with energies of 800, 1000, and 1200 MeV on lead, bismuth, beryllium, carbon, aluminum, and uranium. The results for lead, bismuth, and uranium showed good agreement between the experimental results and the calculated values. For the lighter materials, however, the LCS inconsistently matched the experimental data.

The experimental apparatus used by Belyakov-Bodin, et al. consisted of 24 blocks, each 2.5 cm thick, 20 cm in diameter, and fabricated with internal thermocouples for temperature

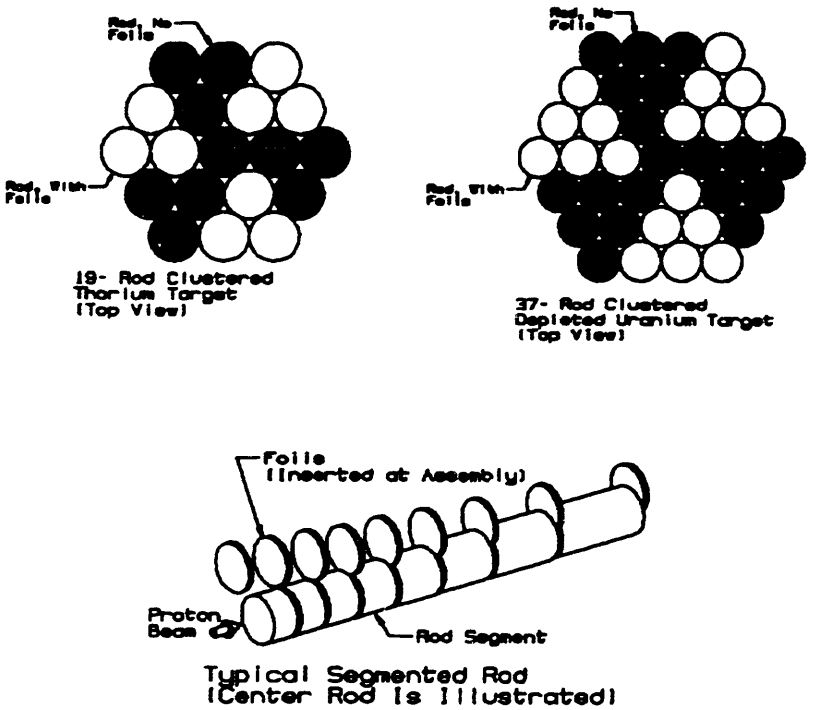

Fig. 3. Illustration of clustered target used in the conversion measurements, the location of the foils in an array, and the foil position within a rod.

measurements. Belyakov-Bodin used two techniques for fabricating the thermocouples into the target. The first, called the whole measuring block technique, involved inserting 12 measuring ends of differential thermocouples into a central disk and sealing them to derive the instantaneous temperature in 2 orthogonal directions at radii of 0.5, 1.3, 2.7, 5.0, and 9.4 cm. They converted temperature to energy deposition by an analytical solution to the linear-heat-transfer equation. Using a second method, named the cut measuring block technique, they divided the block into insulated rings with outer diameters of 2.0 cm, 5.0 cm, 10 cm, and 20 cm. They inserted three ends of differential thermocouples into each ring and directly measured the energy deposition as the integrated temperature variation of a chosen thermally insulated ring.

The LAHET/MCNP geometry, which we set up to model the experimental configuration, consists of a cylinder divided into a total of 48 cells, each 2.5 cm thick, divided into two radial regions ($r<5$ cm and 5 cm$<r<$10 cm), as shown in Fig. 4. We calculated the total energy deposition in each cell by adding the LAHET energy deposition, determined by an HTAPE analysis of the history tape (Type-6 edit with the contributions from nuclear excitation and π^0 decay subtracted), to the coupled neutron-photon energy deposition from MCNP (type 6 tally). To match the quantities determined in the experiment, we determined the total energy deposited to a radius of both 5 cm and 10 cm for each axial cell and divided these values by 2.5 cm to yield the units of energy/unit length. We assumed the axial locations for these values to be the axial midpoints of each cell.

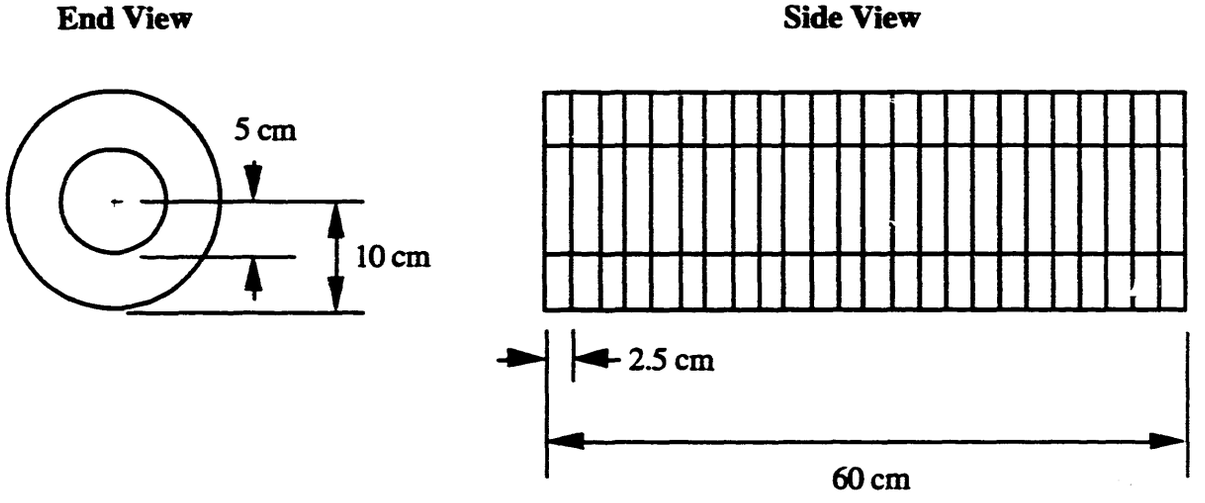

Fig. 4. LCS geometry for energy deposition calculations.

The proton beam distribution in the experiment was approximately Gaussian with FWHM= 2.4 cm that we modeled using a Gaussian distribution with a σ= 1.0213 cm for the LAHET calculations. Belyakov-Bodin et al. stated that in their experiment, the beam had an inclination of 2°±1° and a beam divergence of 0.5°±0.2° for the lead and bismuth experiments. We did not account for these effects in the LAHET calculations.

We used the BERTINI nuclear cascade model for all of the LAHET calculations with many default input parameters. Exceptions included the implementation of the preequilibrium model, the inclusion of elastic scattering, and allowing for the transport of heavy charged particles (for which the BERTINI model only includes slowing down). Belyakov-Bodin, et al. did not give the densities of the materials used in the experiments; therefore, we assumed the densities were the natural densities of the pure materials and used the values shown in Table 3 in the LCS model.

In our study, we investigated both the experimental and LCS values for lead, bismuth, and uranium targets in respect to preselected proton energies and radii. We considered the total energy deposited over the entire length of the targets out to their 5-cm and 10-cm radii (Table 4). We investigated other targets, including beryllium, carbon, and aluminum targets, although we did not investigate their total energy deposition values. The relative errors using LAHET were approximately 0.04 and 0.05 using MCNP with regard to energy deposition in each cell, although some larger values resulted for the lower beam energies at large distances into the target. The relative error for total energy deposition using LAHET was 0.001.

We could not identify specific trends that encompass the results for all of the elements; the results are summarized below for each target material. However, we conclude that, for heavy

Table 3. Assumed Densities for the LCS Calculations

Material	Density (g/cm^3)
Beryllium	1.85
Carbon	1.60
Aluminum	2.70
Lead	11.30
Bismuth	9.80
Uranium	18.90

Table 4. Total Energy Deposited over Axial Length for Radii of 5 cm and 10 cm

Material	Proton Energy (MeV)	Radius (cm)	According to Exp. (MeV)	Quoted Experimental Error (%)	According to Calc. (MeV)	Deviation between Calc. and Exp. (%)*
Lead	800	5	380	7.0	475	25.0
Lead	800	10	460	10.0	523	13.7
Lead	1000	5	450	7.0	540	20.0
Lead	1000	10	520	10.0	608	16.9
Lead	1200	5	530	8.0	611	15.3
Lead	1200	10	600	11.0	687	14.5
Bismuth	800	5	430	4.0	469	9.1
Bismuth	800	10	520	6.0	525	1.0
Bismuth	1000	5	470	4.0	526	11.9
Bismuth	1000	10	570	6.0	600	5.3
Bismuth	1200	5	470	8.0	589	25.3
Bismuth	1200	10	570	10.0	672	17.9
Uranium	800	5	1090	4.4	1205	10.6
Uranium	800	10	1570	5.8	1622	3.3
Uranium	1000	5	1460	6.7	1497	2.5
Uranium	1000	10	2170	7.2	2083	-4.0
Uranium	1200	5	1700	3.5	1784	4.9
Uranium	1200	10	2530	4.1	2540	0.4

*Error defined as (Calc. Value - Exp. Value)/(Exp. Value).

materials, the LCS accurately predicts energy deposition values for both total deposition and deposition at specific locations within the targets with the total energy deposition being correct within approximately 20% and energy deposition values at specific locations being even more accurate. However, for lighter elements, the uncertainty in the predictions is greater. This is partly because the Bertini intranuclear cascade and Dresner evaporation models are statistical in nature and work better for heavier nuclei. Also, nuclear density is not modeled as well for light nuclei.

LANSCE Activation Measurement

To test the accuracy of the LCS coupled with CINDER'90 with regard to predicting residual nuclide activity due to long-term proton bombardment, we performed a comparison of calculational predictions and experimental residual dose rate measurements of the LANSCE target after removal for storage [28]. From November 1985 through October 1990, the LANSCE spallation target received an integrated beam current of about 0.25 amp-hour of 800-MeV protons with a documented operational history. Personnel removed the target on April 7, 1991, and measured gamma dose rates due to the decay of activation products in the target along the outside surface of the target and within the center of the flux trap.

The model we are using for the LCS calculations is a modification of the LANSCE target-moderator-reflector-shield geometry developed by H. G. Hughes and H. Lichtenstein [29–30]. The only modifications we made to this model are the alteration of the cell divisions within the regions of interest (upper tungsten target, lower tungsten target, beryllium, and steel around the central target region) (Fig. 5). We obtained the isotopic concentrations for the LAHET calculations by taking the MCNP material specifications in the Hughes/Lichtenstein model and modifying them when necessary by the isotopic abundances in the Chart of the Nuclides, Thirteenth Edition [31].

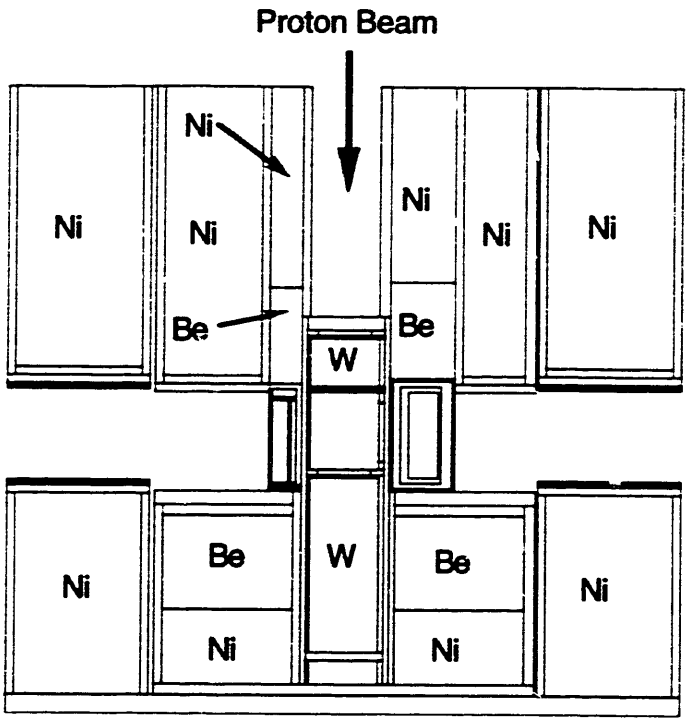

Fig. 5. LCS geometry for LANSCE activation calculations.

In the calculational procedure, we used the LCS to predict the spallation product production and nuclide destruction rates, as well as the flux levels generated in the LANSCE target and surrounding regions during operation. We then used this information to perform subsequent isotopic depletion calculations using CINDER'90. Using CINDER'90, we determined the gamma-source distribution corresponding to the time of the LANSCE target measurements and then inserted the source into the LCS model and transported it using MCNP to determine the dose rates at the measurement locations.

For the LAHET calculation, we ran 50,000 source protons. We then used HTAPE to determine the nuclide production, nuclide destruction, and gas production in the system. We then added the gas production results to the nuclide production files. We transported the resulting generated neutrons in MCNP and tallied the fluxes for the upper tungsten target, the lower tungsten target, and the beryllium and steel, which directly surround the target (everything inside the beryllium sheath). This material was removed as a unit-target-assembly when the measurements were taken.

For the subsequent gamma-transport calculations, we entered the gamma distributions predicted by CINDER'90 (refer to the target/blanket technical report) as homogeneous gamma sources, in the respective regions in which they were generated, by defining a volume for source-point sampling in MCNP and using cell rejection so that particles would only be initiated in the appropriate regions. We used one million source particles for each transport calculation, and we performed a separate calculation for each region so that we could determine the contribution from the various regions. We took point detector tallies in the center of the flux trap and 5.1 cm from the beryllium sheath in the center of the 12.22-cm-wide vertical face, located vertically 11.4, 22.4, and 33.4 cm from the center of the flux trap along the lower tungsten target, and 12.6, 29.5, and 46.4 cm from the center of the flux trap along the upper tungsten target. The tally results were normalized to the total gamma source for each individual region obtained from the CINDER'90 results. These gamma sources are given in Table 5.

Table 5. Decay Gamma-Source Strengths	
Region	**Source Strength (gammas/(s/cm^3))**
Upper Tungsten	4.871e+10
Lower Tungsten	9.680e+09
Beryllium	2.995e+05
Steel	2.095e+09

The greatest error in the LCS results when compared to the experimental values occurred at the bottom of the lower target assembly, where the LCS prediction was 2.4 times greater than the experimental measurement (Table 6). This was also the only value predicted by the LCS that was greater than the measured value. We conclude that the combination of the LCS and CINDER'90 predicted the resulting dose levels surrounding the target to within a factor of about 2, which is quite remarkable for this type of calculation. Furthermore, our problem had significant activation contributions from both spallation (predominantly in the tungsten) and parasitic neutron absorption (primarily in the steel) and illustrates the ability of LCS/CINDER'90 to accurately account for both mechanisms of radionuclide production. Finally, the material composition of the LANSCE target makes this measurement a strong validation for the use of LCS/CINDER'90 for APT activation calculations. Combining LCS with CINDER'90 results in a very useful package for the analysis of APT radionuclide waste streams and subsequent dose levels generated by the activated material.

Table 6. Decay Dose Values Calculated by LCS/CINDER'90 and Experimental Results			
Location	**LCS (kR/h)**	**Measurement (kR/h)**	**Ratio $\left(\frac{\text{LCC}}{\text{Meas.}}\right)$**
Top of Upper Target Assembly	0.07	0.11	0.60
Middle of Upper Target Assembly	0.25	0.39	0.60
Bottom of Upper Target Assembly	0.93	1.30	0.71
Center of Flux Trap	2.21	3.40	0.66
Top of Lower Target Assembly	0.74	1.55	0.47
Middle of Lower Target Assembly	0.65	0.65	0.99
Bottom of Lower Target Assembly	0.46	0.19	2.42

LANSCE Neutron Spectra

Light water. We have measured the neutron flux from the high-intensity H_2O moderator at LANSCE from 0.025 eV to 100 keV [32], and compared the measured values with calculated predictions. The results are shown in Fig. 6 from 0.025 eV to 10 keV. The agreement between calculations and measurements is at the 20% level. This is a very stringent test of the LCS because of the complex geometry and composition of the LANSCE target-moderator-reflector-shield system. (We used the Hughes as-built mockup of the LANSCE target system [29] in our calculations, see Fig. 5.)

Liquid hydrogen. We have also measured the leakage current from the LANSCE liquid para-hydrogen moderator (temperature 20 K) as a function of energy in the range from 0.001 eV to 10 eV. Instead of using gold foil activation analysis, a calibrated low-efficiency neutron beam monitor was used in a time-of-flight experiment to determine the absolute neutron flux. The time distribution (or neutron pulse width) of the leakage current was also measured as a function of energy in range from 0.002 eV to 0.02 eV, but the results are not reported here. The raw data from the beam monitor are shown in Fig. 7.

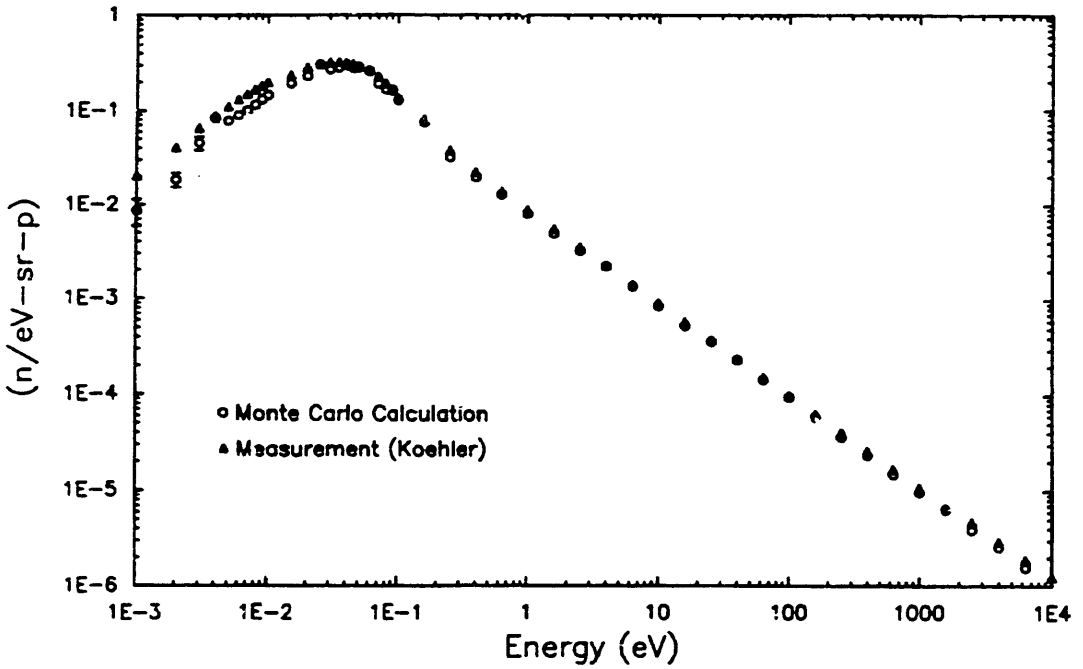

Fig. 6. Calculated and measured neutron energy spectra from the LANSCE high-intensity H_2O moderator.

The neutron counts per channel, N, in the monitor spectrum shown in Fig. 7 can be calculated from the neutron leakage current, $e\Phi(e)$, by

$$N = Conv(t) \times \left(e(t)\Phi(e(t))\right) \tag{1}$$

where e is the energy at time t, and $e\Phi(e)$ is the current in units of neutrons per steradian per proton per lethargy. The function, $Conv(t)$, contains all the experimental parameters (distance, collimation, channel width, efficiency, absorption, number of protons, etc.). In order to obtain an experimental analytical form for $e\Phi(e)$ useful for design, the raw monitor data (dashed line in Fig. 7) were fitted to a parameterized form of the function, $\Phi(e)$, expressed in units of neutrons/sr/p/eV. The current, $\Phi(e)$, is the sum of a thermal contribution and an epithermal contribution and is defined in equation 2.

$$\Phi(e) = \Phi_{th}(e) + \theta_{cut}(e)\Phi_0\Phi_{epi}(e)\exp\left(\frac{abs}{\sqrt{e}}\right) \tag{2}$$

where Φ_0 is an epithermal scale factor. The neutron absorption correction, abs, is included to simulate that the leakage at very low energy will be affected by absorption. The thermal contribution, $\Phi_{th}(e)$, is defined as a Maxwellian distribution

$$\Phi_{th}(e) = J\frac{e}{e_{th}^2}\exp\left(-\frac{e}{e_{th}}\right) \tag{3}$$

where J is the Maxwellian integral, and e_{th} is the Maxwellian temperature in eV. This latter

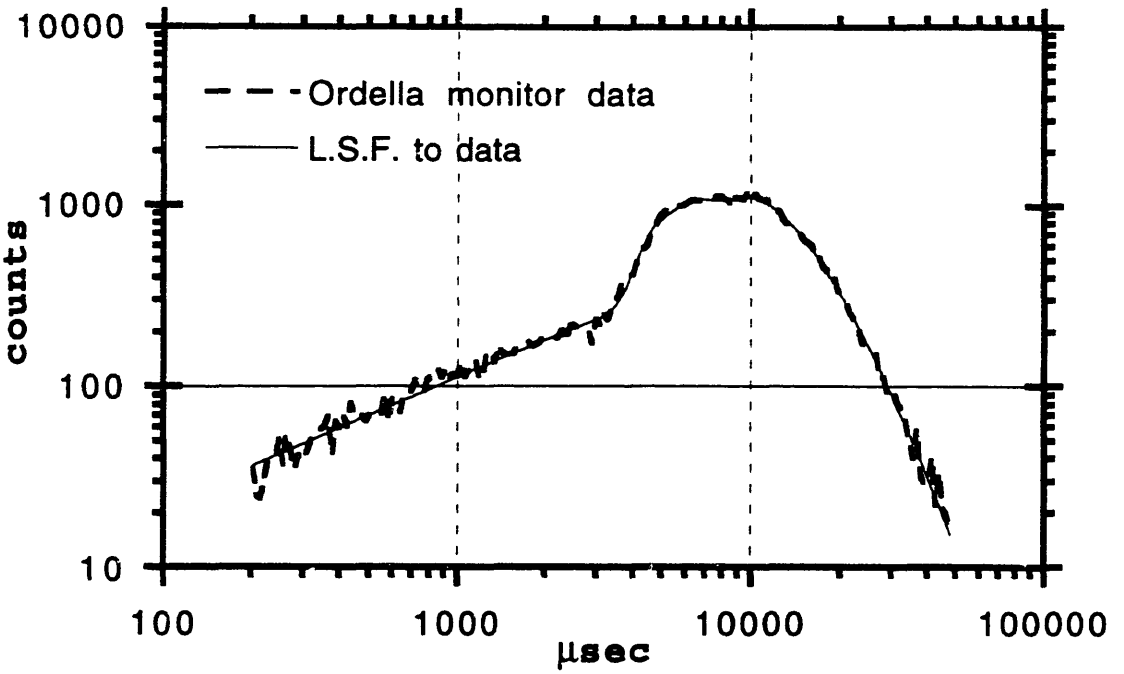

Fig. 7. Monitor spectrum.

parameter can be expected to be somewhat larger than the energy corresponding to 20 K, the temperature of the moderator. The epithermal contribution, $\Phi_{epi}(e)$, joins smoothly on to the thermal part at an energy, e_{cut}, that typically is a few times larger than e_{th}. The joining function, $\Theta_{cut}(e)$, is defined by equation 4. The parameter, β, controls, how rapid Θ_{cut} approaches one.

$$\Theta_{cut}(e) = 1 - \exp(-x)\left(1 + x + 0.5x^2\right)$$

where

$$x = \beta(e - e_{cut}) \qquad e \geq e_{cut}$$
$$x = 0 \qquad e < e_{cut} \tag{4}$$

The Maxwellian maximum for a moderator at 20K should show as a fairly narrow peak at 15000 μsec in the raw monitor data. That peak is clearly not present in Fig. 7. The monitor data show structure in the region between 4000 to 5000 μsec corresponding to neutron energies between 0.015 and 0.020 eV. Since this structure is at much higher energy than expected for both e_{th} and e_{cut}, this structure is associated with the epithermal part, Φ_{epi}, of the neutron leakage. The explanation for the structure is the large change in the neutron scattering cross section for the para-hydrogen molecule at 0.0152 eV (twice the rotational constant for the hydrogen molecule). For neutron energies below 0.0152 eV, only the elastic para-para transition that has a very small neutron cross section is possible. Above 0.0152 eV, the para-ortho transition with a much larger

cross section becomes allowed. The elastic and inelastic contributions to the neutron cross section for para-hydrogen have been calculated in the energy region from 0.0 to 0.04 eV, and the results are shown in Fig. 8. A more complete calculation of the cross section is described by McFarlane [33]. The large decrease in the cross section just below 0.015 eV gives rise to an increase in the leakage. Para-hydrogen becomes almost transparent to neutrons below 0.015 eV. To simulate this change, the traditional functional form for the epithermal part in equation 5 has been multiplied by a switch function, $\rho(e)$.

$$\Phi_{epi}(e) = \rho(e)\Phi_0\left(\frac{e_0}{e}\right)^{1-\alpha} \tag{5}$$

where e_0 is 1 eV. Since the epithermal flux is very nearly inversely proportional to e, the parameter, α, is expected to be small. The switch function, $\rho(e)$, is defined by equation 6.

$$\begin{aligned} &\rho(e) = 1 + \delta_\rho \exp(-x)\left(1 + x + 0.5x^2\right) \\ &\quad \text{where} \\ &\mathrm{x} = \gamma\left(\mathrm{e} - \mathrm{e}_\rho\right) \qquad e \geq e_\rho \\ &\mathrm{x} = 0 \qquad\qquad e < e_\rho \end{aligned} \tag{6}$$

where e_ρ is equal to 0.0152 eV, and γ and δ_ρ are parameters. The monitor counts, N, were fitted by a least squares fitting procedure to the neutron leakage current, $\Phi(e)$, defined by equations 2 through 6. The results for the least squares analysis are given in Table 7.

We are repeating the calculations of the neutron spectra for both the light water and liquid hydrogen moderators using: the most recent LCS model parameters; the inclusion of a proton beam

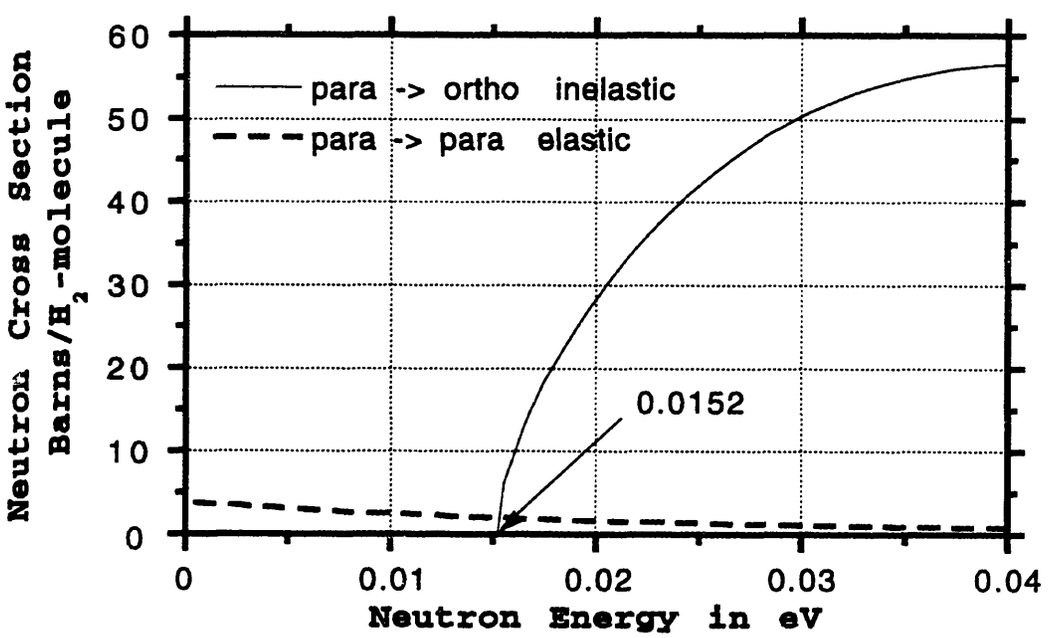

Fig. 8. Calculated hydrogen cross sections.

window in our Monte Carlo simulation; more realistic proton beam profiles; a small addition of ortho-hydrogen; and better statistics. For light water, we use the scattering kernel provided with MCNP, Ref. 11. For liquid hydrogen, we use the scattering kernels for ortho- and para-hydrogen as described by MacFarlane [33].

Figure 9 shows a comparison between the fit to the experimental data and the LCS-calculated neutron beam leakage. The disparity between the calculations and experiment may, in part, be due to the following calculational assumptions and deficiencies:

- the calculation was done for pure para-hydrogen whereas some ortho-hydrogen is present;
- the Monte Carlo computation was not performed with sufficient source particles to yield a small relative error for all energy bins;
- the effects of the proton beam window were not included in the model geometry;
- an "ideal" proton beam profile was used in the calculation, rather than a realistic profile; and
- there may be shortcomings in the scattering kernels with regard to the transition to a $1/E$ spectrum.

The calculations are being redone for both the water and hydrogen moderators with the goal of addressing many of these deficiencies.

Table 7. Parameters for the para-hydrogen moderator leakage current

Maxwellian integral	$J = 0.0101$ n/sr/p
Maxwellian temperature	$e_{th} = 0.00256$ eV
Epithermal scale factor Φ_0 = Leakage current at $E_0 = 1$ eV	$\Phi_0 = 0.00457$ n/sr/p/eV
Epithermal leakage parameter	$\alpha = 0.141$
Parameters for joining function Θ_{cut}	$e_{cut} = 0.00436$ eV $\beta = 645$ eV^{-1}
Parameters for switch function ρ	$\delta_\rho = 1.34 \quad \gamma = 358$ eV^{-1} $\varepsilon_\rho = 0.0152$ eV (fixed)
Absorption correction	$abs = 0.0169$
Goodness of fit	$\chi^2 = 237$ Number of points = 186

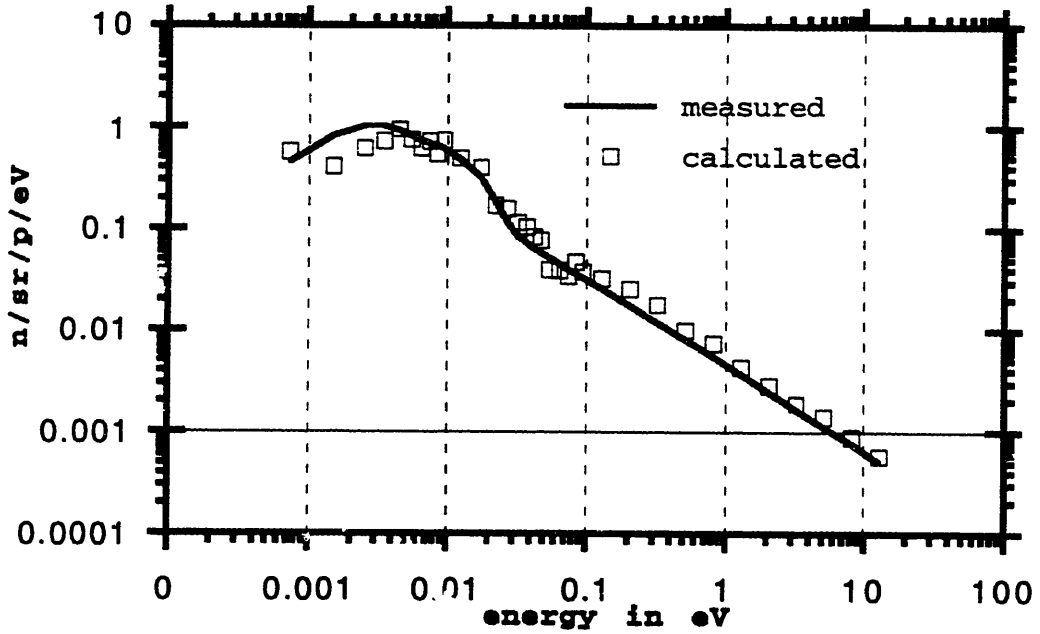

Fig. 9. Comparison of the fit to the measured data and the LCS calculation for the liquid hydrogen moderator.

References

1. Radiation Shielding Information Center, "HETC Monte Carlo High-Energy Nucleon-Meson Transport Code," Oak Ridge National Laboratory report CCC–178 (August 1977).

2. R. E. Prael and H. Lichtenstein, "User Guide to LCS: The LAHET Code System," Los Alamos National Laboratory report LA–UR–89–3014 (September 1989).

3. T. R. England, "CINDER—A One-Point Depletion and Fission Product Program," Bettis Atomic Power Laboratory report WAPD–TM–334 (August 1962, Rev. June 1964).

4. H. W. Bertini, *Phys. Rev.* **188**, 1711 (1969).

5. Y. Yariv and Z. Fraenkel, *Phys. Rev. C* **20**, 2227 (1979).

6. L. Dresner, "EVAP—A Fortran Program for Calculating the Evaporation of Various Particles from Excited Compound Nuclei," Oak Ridge National Laboratory report ORNL–TM–96 (April 1962).

7. K. Chen, et al., *Phys Rev.* **166**, 949 (1968).

8. R. E. Prael and M. Bozoian, "Adaptation of the Multistage Preequilibrium Model for the Monte Carlo Method (I)," Los Alamos National Laboratory report LA–UR–88–3238 (September 1988); R. E. Prael and M. Bozoian, "Adaptation of the Multistage

Preequilibrium Model for the Monte Carlo Method (II),", Los Alamos National Laboratory (to be published).

9. F. Atchison, "Spallation and Fission in Heavy Metal Nuclei under Medium Energy Proton Bombardment," in *Targets for Neutron Beam Spallation Sources*, Jül–Conf–34, Kernforschungsanlage Jülich GmbH (June 1980).

10. J. Barish, T. A. Gabriel, F. S. Alsmiller, and R. G. Alsmiller, Jr., "HET-FIS High-Energy Nucleon-Meson Transport Code with Fission," Oak Ridge National Laboratory report ORNL/TM–7882 (July 1981).

11. J. F. Briesmeister, Ed., "MCNP — A General Monter Carlo Code for Neutron and Photon Transport," Los Alamos National Laboratory report LA–7396–M, Rev. 2 (September 1986).

12. T. R. England, R. Wilczynski, and N. L. Whittemore, "CINDER-7: An Interim Users Report," Los Alamos Scientific Laboratory report LA–5885–MS (April 1975).

13. T. R. England, W. B. Wilson, and M. G. Stamatelatos, "Fission Product Data for Thermal Reactors, Part 1: A Data Set for EPRI–CINDER Using ENDF/B–IV," Los Alamos Scientific Laboratory report LA–6745–MS (December 1976).

14. T. R. England, W. B. Wilson, and M. G. Stamatelatos, "Fission Product Data for Thermal Reactors, Part 2: User Manual for EPRI-CINDER Code and Data," Los Alamos Scientific Laboratory report LA–6746–MS (December 1976).

15. W. B. Wilson, T. R. England, R. J. LaBauve, M. E. Battat, D. E. Wessol, and R. T. Perry, "Status of CINDER and ENDF/B–V Based Libraries for Transmutation Calculations," Proc. Int. Conf. Nuclear Waste Transmutation, Austin, Texas, July 22-24, 1980, p. 673 (March 1981).

16. W. B. Wilson, T. R. England, R. J. LaBauve, and D. C. George, "CINDER-3: Depletion Code for Class VI Computer," Transactions of the American Nuclear Society **46**, 724 (1984).

17. F. M. Mann, "Transmutation of Alloys in MFE Facilities as Calculated by REAC," Hanford Engineering Development Laboratory report HEDL–TME 81–37 (August 1982).

18. F. M. Mann, "REAC-2: A Users Manual and Code Description," Westinghouse Hanford Company report WHC–EP–0282 (December 1989).

19. F. M. Mann, D. E. Lessor, and J. S. Pintler, "REAC Nuclear Data Libraries," Radiation Effects **92**, 207 (1986).

20. F. M. Mann, "Status of Dosimetry and Activation Data," Proceedings of the International Conference on Nuclear Data for Science and Technology, Mito, Japan, May 30-June 3, 1988, p. 1013 (1988).

21. W. B. Wilson and T. R. England, "Nuclear Data Needs for Studies of Accelerator Induced Neutron Transmutation of Nuclear Waste," Proceedings of the Specialists' Meeting on Fission Products and Nuclear Data, May 25–27, 1992, JAERI, Tokai, Japan; organization for Economic Cooperation and Development Nuclear Energy Agency report NEA/NSC/DOC(92)9, pp. 475–481.

22. P. G. Young and W. B. Wilson, "Nuclear Data Requirements for Transmutation," presentation, American Chemical Society, Division of Nuclear Chemistry and Technology Meeting, Denver, Col., March 29, 1993. Los Alamos National Laboratory reports LA–UR–93–994 and –1132.

23. Vassilkov, et al., in Proceeding of the Eleventh Meeting of the International Collaboration on Advanced Neutron Sources, (ICANS–XI), M. Misawa, Ed. (National Laboratory for High-Energy Physics, Tsukuba, 1991), Vol. 1, pp. 340, 612.

24. J. S. Gilmore, G. J. Russell, H. Robinson, and R. E. Prael, "Fertile-to-Fissile and Fission Measurements for Depleted Uranium and Thorium Bombarded by 800-MeV Protons," Nuclear Science and Engineering **99**, 41–52 (1988).

25. V. I. Belyakov-Bodin, et al., "Calorimetric Measurements and Monte Carlo Analyses of Medium-Energy Protons Bombarding Lead and Bismuth Targets," Nuclear Instruments and Methods in Physics Research **A295**, 140–146 (1990).

26. V. I. Belyakov-Bodin, et al., "Calorimetric Measurements and Monte Carlo Analyses of Medium-Energy Protons Bombarding Uranium Targets," Atomic Energy **70**, 339–345 (1991).

27. V. I. Belyakov-Bodin, et al., "Calorimetric Measurements of Medium-Energy Protons Bombarding Beryllium, Carbon, and Aluminum Targets," Nuclear Instruments and Methods in Physics Research **A314**, 508–513 (1992).

28. G. J. Russell, "Predicted LANSCE Target Activity," Los Alamos National Laboratory memorandum LANSCE–92–746, to R. Pynn (October 23, 1992).

29. H. G. Hughes, III, "Monte Carlo Simulation of the LANSCE Target/Moderator/Reflector/Shield Geometry," Advanced Neutron Sources 1988, Proceedings of the 10th Meeting of the International Collaboration of Advanced Neutron Sources (ICANS X) held at Los Alamos, October 3–7, 1988. (IOP Publishing Ltd. Bristol, England 1989).

30. H. G. Hughes and H. L. Lichtenstein, "Enhanced Model of LANSCE Upper Target," Los Alamos National Laboratory memorandum X–6:HGH:HL–92–385, to G. J. Russell (June 11, 1992).

31. *Chart of the Nuclides, Thirteenth Edition*, General Electric Company, Nuclear Energy Operations, San Jose, California (1984).

32. P. E. Koehler, "Measurement of the LANSCE Neutron Flux from 0.025 eV to 100 keV," Los Alamos National Laboratory Report LA–UR–90–290 (1990).

33. R. E. MacFarlane, "Cold Moderator Scattering Kernels," in *Proceedings of the International Workshop on Cold Neutron Sources*, Los Alamos National Laboratory report LA-12146-C (August 1991), pp. 193-216.

END

DATE FILMED

3/14/94